

Realization of complex conjugate media using the real spectra of non-PT-symmetric photonic crystals

Xiaohan Cui,¹ Kun Ding,^{1,2} Jian-Wen Dong,³ and C. T. Chan^{1,*}

¹*Department of Physics, The Hong Kong University of Science and Technology, Clear Water Bay, Kowloon, Hong Kong SAR, China*

²*The Blackett Laboratory, Department of Physics,*

Imperial College London, London SW7 2AZ, United Kingdom

³*School of Physics & State Key Laboratory of Optoelectronic Materials and Technologies, Sun Yat-Sen University, Guangzhou 510275, China*

(Dated: December 24, 2019)

While parity-time (PT)-symmetric systems can exhibit real spectra in the exact PT-symmetry regime, the PT-symmetry is actually not a necessary condition for the real spectra. Here we show that non-PT-symmetric photonic crystals carrying Dirac-like cone dispersions can always exhibit real spectra as long as the average non-Hermiticity strength within the unit cell for the eigenstates is zero. By building a non-Hermitian Hamiltonian model, we find that the real spectra of the non-PT-symmetric system can be explained using the concept of pseudo-Hermiticity. We demonstrate using effective medium theories that in the long-wavelength limit, such non-PT-symmetric photonic crystals behave like the so-called complex conjugate medium (CCM) whose refractive index is real but whose permittivity and permeability are complex numbers. The real refractive index for this effective CCM is guaranteed by the real spectrum of the photonic crystals and the complex permittivity and permeability comes from the non-PT-symmetric loss-gain distributions. We show some interesting phenomena associated with the CCM, such as the lasing effect.

I. INTRODUCTION

Hermitian Hamiltonian can describe ideal closed physical systems, in which the total energy is conserved, and eigenfrequencies are purely real. However, non-conservative elements are ubiquitous in classical wave systems, and we need to introduce the concept of non-Hermiticity to describe such systems. In the past decades, there is a surge of interest in studying the physics of non-Hermitian systems¹⁻⁷ and the parity-time (PT)-symmetric system, which was first introduced in quantum mechanics¹, is the most popular one. A Hamiltonian H is said to be PT-symmetric if $[H, PT] = 0$, where the operator P represents a space reflection, and the operator T represents a time reversal. PT-symmetric systems have been realized in optics and photonics⁸⁻¹⁰. In an optical system, the loss-gain (represented by the imaginary part of the refractive index) distribution is PT-symmetric, if the complex-valued refractive index satisfies $n(x) = n^*(-x)$.

The most intriguing property of a PT-symmetric Hamiltonian is that it can exhibit real spectra in the exact PT-symmetry regime². As we change the parameters of the Hamiltonian, such as the loss-gain strength, it may go into the broken PT-symmetry regime, and the eigenvalues form complex conjugate pairs. The symmetry-breaking point, marking the phase transition in the eigenvalue spectrum, is the exceptional point (EP)^{11,12}. However, PT-symmetry is not a necessary condition for achieving a real spectrum¹³ and some studies about realizing real spectra in non-PT-symmetric systems have been presented recently¹⁴⁻¹⁸. It has been proved that the necessary condition for the real spectrum is pseudo-Hermiticity¹³. A Hamiltonian H satisfying $\eta H \eta^{-1} = H^\dagger$

, where η is an invertible linear Hermitian operator, is defined as pseudo-Hermitian Hamiltonian (see Supplementary Note 1 for details). Real spectra realized in non-PT-symmetric systems can be explained using the concept of pseudo-Hermiticity.

Achieving the real spectra in a non-PT-symmetric PC is highly desirable because from an effective medium theory (EMT) point of view¹⁹, realizing the real spectra in certain regions of the Brillouin zone can lead to new applications. For example, one can then realize a complex conjugate medium (CCM)²⁰⁻²², which carries many unusual phenomena, including coherent perfect absorption and lasing²³, and negative refraction²⁴. The refractive index of the CCM is a real number, but their permittivity and permeability can both be complex numbers in general²⁰. From the EMT point of view, achieving a complex conjugate medium using a PC requires the non-Hermitian PC to exhibit real frequency bands near the Brillouin zone center (Γ point) because the effective refractive index is real.

To understand the underlying physics, we build a two-band non-Hermitian Hamiltonian model for the non-PT-symmetric photonic crystals. We show that the model Hamiltonian is pseudo-Hermitian as long as the average non-Hermiticity strength (to be defined below) within the unit cell for the relevant states is zero and this condition can always be achieved in PCs that have Dirac-like cone dispersions. Consequently, real spectra can be realized in a particular frequency range, implying that the effective refractive index is real. In the long-wavelength limit, the scattering properties of such an inhomogeneous PC behave indeed like a homogeneous complex conjugate medium.

II. THE TWO-BAND NON-HERMITIAN HAMILTONIAN MODEL

As shown in the inset of Figure 1A, we consider a two-dimensional (2D) PC with rods arranged in a square lattice in the $x-y$ plane. Within the unit cell with a lattice constant a , the rod (domain A, the blue region) having a radius r_c , and relative permittivity $\varepsilon_A = \varepsilon_{cr} + i\gamma$ is embedded in a background medium (domain B, the grey region) with relative permittivity $\varepsilon_B = \varepsilon_{br} + i\ell_r\gamma$. We set $\varepsilon_{br} = 1$ in the calculation and the relative permeability μ of both media as 1.0. The positive (negative) sign of γ indicates that the rod consists of a lossy (active) medium. A positive sign of ℓ_r indicates that the rod and background are either both lossy or both active, while a negative sign means that one is lossy and the other is active.

We study the PC in the transverse-magnetic (TM) polarization, where the electric field $\mathbf{E} = E\hat{z}$ is normal to the $x-y$ plane, and the electromagnetic waves propagate in the plane. As shown in Figure 1A, in the Hermitian limit ($\gamma = 0$), this system has a Dirac-like cone dispersion²⁵ at the Brillouin zone center induced by accidental degeneracy. Compared with the Dirac cone of graphene system at the Brillouin zone corner, there is an additional flat band in the Dirac-like cone. It has been experimentally confirmed that the radiation existing in an open system can spawn rings of EPs in the wave vector space $\mathbf{k} = (k_x, k_y)$ out of Dirac-like cones²⁶; but imaginary parts of the eigenfrequencies are negative because of radiation loss. Now we will see whether we can tune the bands outside the ring to become real spectra by adding gain into the system. In principle, the eigenfrequency and eigenfunction of Bloch states for this non-Hermitian 2D PC can be obtained by numerically solving the Helmholtz equation²⁷. However, to study the band structure of the non-Hermitian PC analytically, we construct a model Hamiltonian using Hermitian systems Bloch states obtained at a fixed value of \mathbf{k} as the bases, and obtain a generalized eigenvalue problem as (see Supplementary Note 3 for details)²⁸,

$$H_2 p_{\mathbf{k}n} = (\omega_{\mathbf{k}n}/c)^2 H_1 \cdot p_{\mathbf{k}n}, \quad (1)$$

where c is the speed of light, and $\omega_{\mathbf{k}n}$ and $p_{\mathbf{k}n}$ are the eigenfrequencies and eigenvectors of the non-Hermitian system ($\gamma \neq 0$). The matrices in Eq. (1) are $(H_1)_{mm'} = \delta_{mm'} + i\gamma(F_{A,mm'} + \ell_r F_{B,mm'})$, and $(H_2)_{mm'} = \delta_{mm'}(\omega_{\mathbf{k}m}^{(0)}/c)^2$. $\omega_{\mathbf{k}m}^{(0)}$ is the eigenfrequency of the Hermitian PC. To characterize the eigenmode profiles, we introduce a quantity

$$F_{\Omega,mm'} = \int_{\Omega} d^2r u_{\mathbf{k}m}^{(0)*}(\mathbf{r}) u_{\mathbf{k}m'}^{(0)}(\mathbf{r}), \quad (2)$$

where Ω denotes the rod ($|\mathbf{r}| < r_c$) or air ($|\mathbf{r}| > r_c$) domain. $F_{\Omega,mm'}$ ($m \neq m'$) expresses the overlapping between two different eigenmodes in the domain Ω and

$F_{\Omega,mm}$ expresses the amplitude distribution of the eigenmode m in the domain Ω . $u_{\mathbf{k}m}^{(0)}(\mathbf{r})$ are the eigenvectors of the Hermitian PC ($\gamma = 0$) and satisfy the orthonormal relation

$$\varepsilon_A F_{A,mm'} + \varepsilon_B F_{B,mm'} = \delta_{mm'}, \quad (3)$$

where $\varepsilon_A = \varepsilon_{cr}$ denotes the relative permittivity of the rod domain and $\varepsilon_B = \varepsilon_{br} = 1$ represents the relative permittivity of the air domain. For convenience, we can omit the subscript \mathbf{k} for simplicity and rewrite Eq. (1) as $H \cdot p_n = W_n p_n$, where $W_n = (\omega_n/c)^2$ and $H = H_1^{-1} \cdot H_2$.

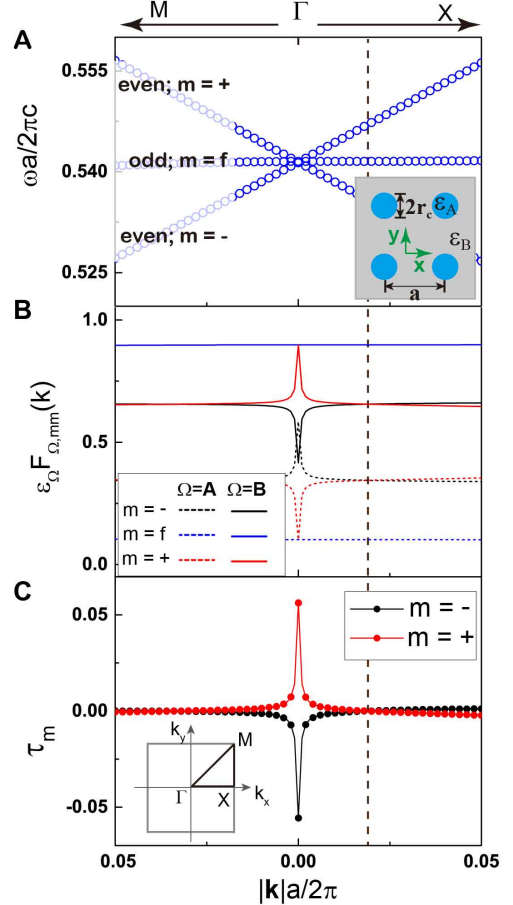


FIG. 1. Properties of the Dirac-like cone. (A) Band dispersions of Hermitian PC ($\gamma = 0$) calculated using COMSOL. (B) Eigenmode profiles of the upper bands $m = +$ (even mode), flat band $m = f$ (odd mode), and lower band $m = -$ (even mode). (C) The average non-Hermiticity τ_m when the gain-to-loss ratio $\ell_r = -0.15235$. The vertical dashed line denotes the intersection: $F_{\Omega,++} = F_{\Omega,--}$. The inset in (A) shows a schematic of the 2D PC, constructed with cylinders (the blue areas) and the grey area denotes air. The inset in (C) represents the first Brillouin zone of the square lattice. The parameters used are $r_c = 0.1999a$, $\varepsilon_A = 12.5 + i\gamma$, and $\varepsilon_B = 1 + i\gamma\ell_r$.

From Eq. (2), we know that the function $F_{\Omega,mm'}$ involves the spatial integrations of eigenfunctions of Hermitian

tian systems, and hence the symmetry of the eigenmode profile plays an important role here. In our system, we choose the center of the rod as origin. The even/odd symmetry characters are labeled in Figure 1A^{27,29}. Since the two linearly dispersive bands ($m = \pm$) are even while the flat band ($m = f$) is an odd mode, the matrix elements $F_{\Omega,+f}$ and $F_{\Omega,-f}$ are all zero, implying that there is no coupling between the flat band and the linear bands. Therefore, we can decouple the flat band from the Hamiltonian model, and write the Hamiltonian as a 2×2 matrix (see Supplementary Note 3 for details),

$$H = \frac{1}{\beta} \begin{pmatrix} W_-^{(0)}(1 + i\gamma\tau_-) & -i\gamma\kappa W_+^{(0)} \\ -i\gamma\kappa^* W_-^{(0)} & W_+^{(0)}(1 + i\gamma\tau_+) \end{pmatrix}, \quad (4)$$

where $\beta = 1 + i\gamma(\tau_- + \tau_+) + \gamma^2(|\kappa|^2 - \tau_- \tau_+)$. In Eq. (4),

$$\tau_m = F_{A,mm} + \ell_r F_{B,mm}, \quad (m = \pm) \quad (5)$$

is a real number, representing the average non-Hermiticity of state m within the primitive unit cell, and

$$\kappa = F_{A,-+} + \ell_r F_{B,-+}, \quad (6)$$

is a complex number, representing an overlapping between the two eigenmodes. According to Eq. (5), the values of τ_{\pm} depend not only on the distributions of non-Hermiticity (described by ℓ_r) in the unit cell but also on the eigenmode profiles (as described by $F_{\Omega,mm}$). The average non-Hermiticity τ_{\pm} is very important, because it can determine whether we can obtain the real spectra in a non-Hermitian PC (see Supplementary Note 4). To see this, we set the average non-Hermiticity $\tau_{\pm} = 0$, and then the Hamiltonian (4) becomes

$$H = \frac{1}{\beta} \begin{pmatrix} W_-^{(0)} & -i\gamma\kappa W_+^{(0)} \\ -i\gamma\kappa^* W_-^{(0)} & W_+^{(0)} \end{pmatrix}, \quad (7)$$

where $\beta = 1 + \gamma^2|\kappa|^2$ is a real number.

Near the Γ point, we can expand the eigenfrequencies of the two linear bands for a small $k \equiv |\mathbf{k}|$ into

$$W_{\pm}^{(0)} = (\omega_d/c \pm v_g k/c)^2 \approx W_d \pm C_g k, \quad (8)$$

where $C_g = 2\omega_d v_g/c^2$, $W_d = (\omega_d/c)^2$, and ω_d is the Dirac-like point frequency. The band slope v_g can be obtained from numerical results in Figure 1A, where we assume v_g is a constant along all directions in the wave vector space, which is an excellent approximation of a conical dispersion at $k = 0$ for a system with C_{4v} symmetry²⁹. The corresponding eigenvalues are

$$W_{\pm} = \frac{1}{\beta} \left(W_d \pm \sqrt{(C_g k)^2 (1 + \gamma^2|\kappa|^2) - \gamma^2|\kappa|^2 W_d^2} \right). \quad (9)$$

EPs appears when the value under the square root is zero and form a ring in the wave vector space with a radius

$k_c = k_b(1 + |\gamma\kappa|^{-2})^{-\frac{1}{2}} \leq k_b$, where $k_b = \omega_d/2v_g$ is the upper bound of the rings radius. This means that the radius of the EP ring in \mathbf{k} space cannot exceed k_b for any value of γ . In general, $|\kappa|$ is a small number, and the radius of the ring can be reduced to $k_c \approx k_b |\gamma\kappa|$. The eigenvalues are real outside the ring ($k > k_c$) and form complex conjugate pairs inside the ring ($k < k_c$). Therefore, by setting the average non-Hermiticity $\tau_{\pm} = 0$, we can obtain a real spectrum in a certain region (Supplementary Fig. S1b gives a schematic of the band dispersions).

Before proceeding to the next subsection, the Hamiltonian (7) deserves more comments. Using the linear operator

$$\eta = \begin{pmatrix} W_-^{(0)} & 0 \\ 0 & -W_+^{(0)} \end{pmatrix}, \quad (10)$$

the Hamiltonian (7) satisfies

$$\eta H(\gamma) \eta^{-1} = H(\gamma)^\dagger = H(-\gamma), \quad (11)$$

implying the Hamiltonian is pseudo-Hermitian, and the operator η transform the system with non-Hermiticity γ into its complex conjugate-paired system $-\gamma$. Unlike the traditional PT-symmetric system, the loss-gain distribution of our PC system is not PT-symmetric in real space, $n(x) \neq n^*(-x)$.

III. RESULTS

A. Realizing the pseudo-Hermitian condition using a Dirac-like cone

The previous section shows that by setting the average non-Hermiticity $\tau_{\pm} = 0$, the non-Hermitian Hamiltonian will become pseudo-Hermitian and we can obtain the real spectra. For a PT-symmetric PC, $\tau_{\pm} = 0$ is automatically satisfied since the distributions of loss and gain within the unit cell are equal (see Supplementary Note 2 for details)³⁰. However, for a non-PT-symmetric PC, achieving $\tau_{\pm} = 0$ is not an easy task. Now we will show that for a PC exhibiting a Dirac-like cone in the Brillouin zone center, we can always achieve the pseudo-Hermitian condition $\tau_{\pm} = 0$.

The eigenmode $u_{\mathbf{k}\pm}^{(0)}(\mathbf{r})$ in the quantity $F_{\Omega,mm'}$ depends on the structural details (such as the filling ratio r_c and the contrast between ε_A and ε_B) of the PC and can be computed numerically using COMSOL. Substituting the orthonormal relationship Eq. (3) into the pseudo-Hermitian criteria $\tau_{\pm} = 0$, we solve a specific value of the loss-gain ratio ℓ_r

$$\ell_r = \frac{-F_{A,mm}}{F_{B,mm}} = \frac{-F_{A,mm}\varepsilon_B}{1 - F_{A,mm}\varepsilon_A}, \quad (12)$$

for both $m = +$ and $m = -$. Equation (12) shows that to determine the value of ℓ_r , we must tune the system parameters so that the system satisfies $F_{\Omega,++} = F_{\Omega,--}$.

The band dispersions near the Dirac-like cone are shown in Figure 1A, and the quantities $\varepsilon_\Omega F_{\Omega,mm}$ of the three bands are plotted in Figure 1B. We can see that there is an intersection ($F_{\Omega,++} = F_{\Omega,--}$) at $k_x a/2\pi = 0.019$ (marked by the dashed line), and then Eq. (12) can be used to determine the gain-to-loss ratio, which is found to be $\ell_r = -0.15235$. Physically, the existence of such an intersection is guaranteed by the band inversion in the Dirac-like cone²⁵. The condition $F_{\Omega,++} = F_{\Omega,--}$ can always be achieved near the Dirac-like cone (see Supplementary Note 6 and Supplementary Figure S1 for details), and therefore, $\tau_\pm = 0$ is realized at $k_x a/2\pi = 0.019$ as shown in Figure 1C. Note that the quantity $F_{\Omega,mm}$ should be a function of \mathbf{k} , but near the Dirac-like cone (except the Γ point), this quantity is almost a constant (as shown in Figure 1B), because the eigenmodes of the same point group are almost unchanged when the change of \mathbf{k} is small. We can therefore assume the values τ_m , and κ are independent of \mathbf{k} in the considered Brillouin zone region. As shown in Figure 1C, by tuning $\ell_r = -0.15235$, we can obtain $\tau_\pm \approx 0$ near the Dirac-like cone (except very close to the Γ point, where $\tau_- \approx -\tau_+$). We can demonstrate that the pseudo-Hermitian condition at the Γ point is $\tau_- = -\tau_+$, which is less demanding than other points, because the symmetry at the Γ point is higher than that at other \mathbf{k} points (see Supplementary Note 5 for details). So the pseudo-Hermitian criterion is approximately fulfilled for all the \mathbf{k} points near the Dirac-like cone.

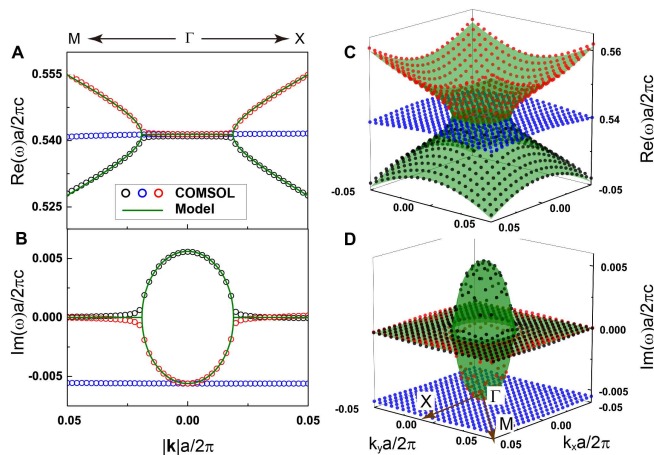


FIG. 2. Band dispersions of the pseudo-Hermitian bands. The real parts (A, C) and imaginary parts (B, D) of the complex eigenfrequencies along the $M - \Gamma - X$ direction and in the 2D Bloch \mathbf{k} space. The open circles and solid dots are calculated using COMSOL, while the green solid lines and green surfaces are calculated using the analytical model ($v_g = 0.295c$ and $|\kappa|^2 = 0.00318$). The bands outside the ring are entirely real. The parameters of the 2D PC are $r_c = 0.1999a$, $\epsilon_A = 12.5 + i\gamma$, $\epsilon_B = 1 + i\gamma\ell_r$, $\gamma = +0.367$, and $\ell_r = -0.15235$.

Now we can calculate the band structures of a PC with

loss-gain ratio $\ell_r = -0.15235$ to verify the validity of the pseudo-Hermitian Hamiltonian shown in Eq. (7). We choose a non-Hermitian strength $\gamma = +0.367$ and plot the complex band structure along the $M - \Gamma - X$ direction in Figures 2A and 2B. The analytical results are shown by the solid green lines and the numerical results calculated using COMSOL by open circles. The validity of our non-Hermitian Hamiltonian model is demonstrated by the good agreement between the two sets of results. We can see that EPs appear in both the $\Gamma - X$ and $\Gamma - M$ directions. To show that these EPs form a ring in \mathbf{k} space, we plot the three-dimensional complex band structure in Figures 2C and 2D using Eq. (9) and COMSOL, as shown by green surfaces (analytical results) and filled dots (numerical results), respectively. The analytical model (9) predicts that $k = k_c = 0.019(2\pi/a)$ form a ring of EPs, which is verified by the COMSOL results. The eigenfrequencies inside the ring form complex-conjugate pairs, and outside the ring, we obtain the entirely real spectra.

However, entirely real spectra does not mean loss-gain compensation. To see this, we compare the system with non-Hermiticity $\gamma_+ = +0.367$ with its complex conjugate-paired system $\gamma_- = -0.367$. If we replace γ_+ by γ_- , the eigenfrequencies described by Eq. (9) are the same but the Hamiltonians (7) are different as described by Eq. (11). In other words, these two systems (γ_+ and γ_-) possess the same band dispersion, but the eigenfunctions are different (see Supplementary Note 7 for details) and hence they can display different scattering behaviors, as we will show later.

B. Real spectra and complex conjugate media

The optical properties of a Hermitian PC carrying a Dirac-like cone in the Brillouin zone center can be described using an effective refractive index medium in which the effective permittivity and permeability are simultaneously zero at the Dirac-like point frequency. We have shown in the previous subsection that by setting the average non-Hermiticity as zero, the spectra are real outside the ring of the EPs. It is interesting to see what type of effective medium corresponds to the non-PT-symmetric PC with real spectra. In this section, we will establish the EMT of non-Hermitian PC for describing the physics near the Γ point and study the related scattering properties.

We calculate the effective parameters using a boundary field averaging method³¹. Assuming that the wave $\mathbf{k} = k\hat{x}$ propagates along the x direction, we define $Z = E_z/H_y = -\omega\mu/k = -k/(\omega\varepsilon)$ for a plane wave traveling in a homogeneous medium to express the ratio between the electric fields and the magnetic fields. For the inhomogeneous PC system, the average field ratio is defined as

$$Z^{\text{PC}} = \frac{\int_I E_z^{\text{PC}} dy}{\int_I H_y^{\text{PC}} dy}, \quad (13)$$

where E^{PC} and H^{PC} are obtained from the eigenfields at the incident boundary I (the boundary of the unit cell along y direction). When we calculate effective parameters of the non-Hermitian PC as functions of frequency, the frequencies should take real-valued numbers. Because in actual experiments, the incident light comes with a real frequency. Therefore, within the PC, the eigenfields E^{PC} and H^{PC} are obtained by solving the complex-valued $\mathbf{k}(\omega)$ vs. real-valued ω band structures³². In Figure 3A, we plot the complex-valued $\mathbf{k}(\omega)$ band structure of the non-Hermitian 2D PC calculated using COMSOL. We note that the imaginary parts of the bands (red lines) are almost zero, and for real bands, the complex-valued $\mathbf{k}(\omega)$ band structure should agree well with the complex-valued $\omega(\mathbf{k})$ vs. real-valued \mathbf{k} band structure (see Supplementary Figure S7 for details). In Figure 3B, we plot Z^{PC} defined in Eq. (13) for the bands with positive (dashed lines) and negative (solid lines) wave vectors respectively in Figure 3A. The effective permittivity and permeability can be calculated as follows:

$$\varepsilon_e = \frac{-k}{\omega \varepsilon_0 Z^{\text{PC}}}, \quad \mu_e = \frac{-k}{\mu_0 \omega} Z^{\text{PC}}. \quad (14)$$

We plot the real and imaginary parts of $\varepsilon_e(\mu_e)$ by squares (stars) in Figs. 3C and 3D, respectively. Note that the effective parameters obtained from the two bands (\mathbf{k} and $-\mathbf{k}$) are the same.

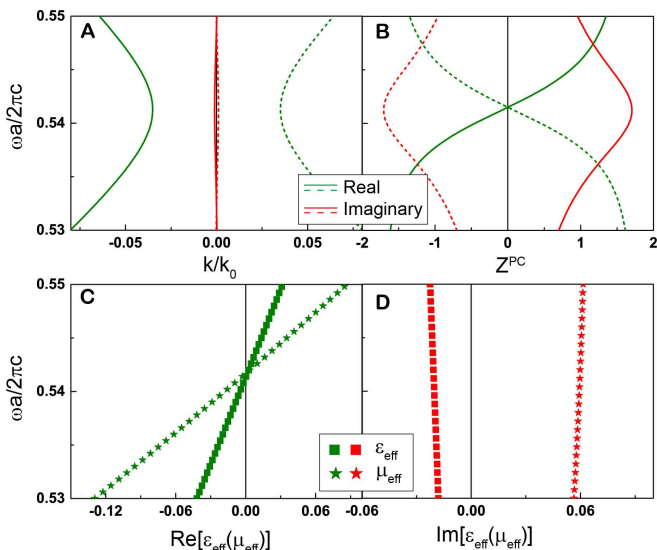


FIG. 3. Effective parameters obtained from the real spectra shown in Figure 2. (A) The complex-valued $\mathbf{k}(\omega)/k_0$ band and (B) the averaged field ratio Z^{PC} calculated numerically from COMSOL. The bands with positive and negative wave vectors are represented by dashed and solid lines respectively. The real (green) and imaginary parts (red) of the effective parameters ε_e and μ_e are plotted in squares and in stars, respectively in (C) and (D).

It is known that for the Hermitian case, the effective parameters of the PC are real and approach zero near the

Dirac-like point frequency, indicating that the PC can be treated as a zero refractive index medium²⁵. When we introduce loss and gain into the PC, the effective parameters ε_e and μ_e obtain imaginary parts as shown in Figure 3D. However, we note that the effective refractive index $n_e^2 = \varepsilon_e \mu_e = (k/k_0)^2$ is a real number, where k_0 is the wave vector in air. This automatically indicates the inhomogeneous PCs behaves like the homogeneous CCM whose refractive index is real but whose permittivity and permeability are complex numbers. The real effective refractive index does not necessarily imply a simple loss-gain compensation, because ε_e and μ_e have imaginary parts. And it can be proved that $\varepsilon_e^{(\gamma_+)} = \varepsilon_e^{(\gamma_-)*}$ and $\mu_e^{(\gamma_+)} = \mu_e^{(\gamma_-)*}$ (see Supplementary Note 8 for details).

The complex conjugate-paired systems (γ_+ and γ_-) have dramatically different effects on the scattering properties of electromagnetic waves. To demonstrate this, we consider a slab with thickness d formed by the homogeneous effective media (EM) with the parameters ε_e and μ_e , as shown in Figure 4A. We assume that plane waves propagate along the x direction with an electric field polarized along the z direction and that the EM slab (the blue region) is embedded in air (the grey region). The electric field in the air can be written as $E(x) = a_1 \exp(ik_0x) + b_1 \exp(-ik_0x)$ for $x < -d/2$, and as $E(x) = b_2 \exp(ik_0x) + a_2 \exp(-ik_0x)$ for $x > d/2$. The amplitudes of incoming-propagating waves $(a_1, a_2)^T$ and outgoing-propagating waves $(b_2, b_1)^T$ are related by a scattering matrix²³

$$S = \begin{pmatrix} t & r \\ r & t \end{pmatrix} = \frac{1}{M_{22}} \begin{pmatrix} 1 & M_{12} \\ M_{12} & 1 \end{pmatrix}, \quad (15)$$

where r and t represent the transmission and reflection coefficients of the slab for normal incident plane waves. The elements in S are

$$M_{12} = i \frac{n_e^2 - \mu_e^2}{2n_e \mu_e} \sin(kd), \quad (16)$$

$$M_{22} = e^{(ik_0d)} \left[\cos(kd) - i \frac{n_e^2 + \mu_e^2}{2n_e \mu_e} \sin(kd) \right], \quad (17)$$

where $k = k_0 n_e$ is the wave vector in the slab. The corresponding eigenvalues of the S matrix are

$$\lambda_{\pm} = \frac{1}{M_{22}} [1 \pm M_{12}]. \quad (18)$$

These eigenvalues can be used to determine the S matrix poles ($1/\text{Max}|\lambda_{\pm}| \rightarrow 0$) where lasing occurs. For a slab composed of CCM [$\text{Im}(n_e) = \text{Im}(k/k_0) = 0$], kd is a real number. For the S matrix to have poles, we require $M_{22} = 0$, and therefore we obtain

$$\frac{n_e^2 + \mu_e^2}{n_e \mu_e} = -2i \cot(kd). \quad (19)$$

To satisfy Eq. (19), μ_e must be an imaginary number. Figures 3C and 3D show the effective parameters of PCs

with non-Hermiticity $\gamma_+ = +0.367$. We find $\text{Re}[\mu_e^{(\gamma_+)}] = 0$ at $\omega a/2\pi c = 0.5416$, and we can solve Eq. (19) to obtain the slab thickness $d/a = 17.4$. For PCs with non-Hermiticity $\gamma_- = -0.367$, the effective parameters are $\varepsilon_e^{(\gamma_+)} = \varepsilon_e^{(\gamma_-)*}$ and $\mu_e^{(\gamma_+)} = \mu_e^{(\gamma_-)*}$, and we can solve the slab thickness $d/a = 8.9$.

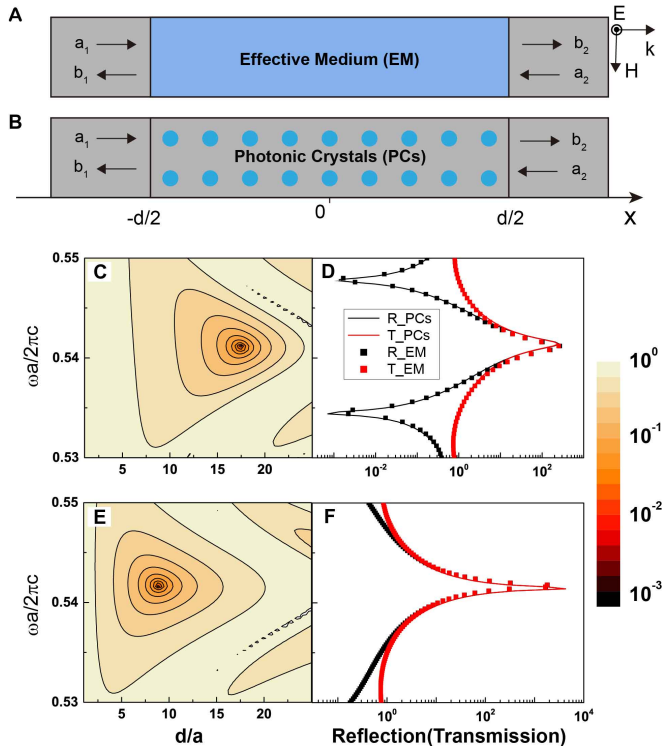


FIG. 4. Scattering properties of the CCM with effective parameters shown Figure 3. The schematics of wave scattering in a (A) EM slab and (B) PCs slab. The contour plot of the value $1/\text{Max}|\lambda_{\pm}|$ in the (ω, d) plane for the EM slab with parameters (C) $\varepsilon_e^{(\gamma_+)}$, $\mu_e^{(\gamma_+)}$ and (E) $\varepsilon_e^{(\gamma_-)}$, $\mu_e^{(\gamma_-)}$. The black and red solid lines represent respectively the reflection R and transmission T for PCs slab, while the black and red squares represent EM slab. The non-Hermiticity strength of PCs are (D) $\gamma_+ = +0.367$ and (F) $\gamma_- = -0.367$. The slab thicknesses are $d/a = 17$ in (b) and $d/a = 9$ in (d).

Figures 4C and 4E show the contour plots of $1/\text{Max}|\lambda_{\pm}|$ in the $(\omega a/2\pi c, d/a)$ plane for EM slab with $(\varepsilon_e^{(\gamma_+)}, \mu_e^{(\gamma_+)})$ and $(\varepsilon_e^{(\gamma_-)}, \mu_e^{(\gamma_-)})$ respectively. To verify the scattering poles ($1/\text{Max}|\lambda_{\pm}| \rightarrow 0$), in Figure 4B, we plot the transmission $T = |t|^2$ and reflection $R = |r|^2$ of slabs formed by homogeneous EM by squares and PCs by solid lines. The schematic of the one-dimensional scattering problem of slab formed by PCs is plotted in Figure 4B. We set the thickness of the slab $d/a = 17$, because the thickness of the slab formed by PCs must be an integer. The good agreement between the EM and PCs re-

sults shows that the effective parameters shown in Figs. 3C and 3D essentially reproduce the physics. We can see that the system indeed has the transmission and reflection singularities at $\omega a/2\pi c = 0.5416$ in Figure 4D. This indicates that we can observe the poles of the S matrix from the transport configuration. Similarly, the pole in Figure 4E at $d/a = 8.9$ and $\omega a/2\pi c = 0.5416$ for $(\varepsilon_e^{(\gamma_-)}, \mu_e^{(\gamma_-)})$ is also verified by the transmission and reflection singularities in Figure 4F, where $d/a = 9$. When we change the sign of γ , the real bands of the PCs remains almost the same but the non-Hermitian PCs do not have time reversal symmetry. Although the refractive index satisfies $n_e^{(\gamma_+)} \approx n_e^{(\gamma_-)}$, the scattering phenomena change drastically because the effective permeability (or impedance) has imaginary parts, and $\mu_e^{(\gamma_+)} \neq \mu_e^{(\gamma_-)}$. This illustrates that the S matrix poles depend not only on the refractive index but also on the permeability as shown in Eq. (19). The sum of the transmission and reflection is not equal to unity, although the slabs effective refractive index is real. A real refractive index does not necessarily imply energy compensation. The focusing effect of our PCs as a lens is also different for these complex paired systems (see Supplementary Note 9 for details).

IV. DISCUSSION

In this work, we find that a non-PT-symmetric PC can have real spectra when the average non-Hermiticity within the unit cell is zero. We showed that the pseudo-Hermitian condition ($\tau_{\pm} = 0$) can always be fulfilled in two-component PCs carrying Dirac-like cones with bands arising from monopolar and dipolar resonances. These non-Hermitian PCs carrying Dirac-like cones can be used to realize CCM near the Dirac-like point frequency, where a real spectrum guarantees a real refractive index and the non-Hermiticity guarantees complex permittivity and permeability.

V. ACKNOWLEDGEMENT

This work is supported by the Research Grants Council, University Grants Committee, Hong Kong, through grants No. AoE/P-02/12, N_HKUST608/17, 16303119 and C6013-18G and by the National Natural Science Foundation of China (Grant Nos. 11761161002, 61775243). K.D. acknowledges funding from the Gordon and Betty Moore Foundation. We would like to thank Prof. Zhao Qing Zhang and Dr. Ruoyang Zhang for helpful discussions.

* phchan@ust.hk

¹ Carl M. Bender and Stefan Boettcher. Real Spectra in Non-Hermitian Hamiltonians Having P T Symmetry.

- Physical Review Letters*, 80(24):5243–5246, June 1998.
- ² Carl M. Bender, Dorje C. Brody, and Hugh F. Jones. Complex Extension of Quantum Mechanics. *Physical Review Letters*, 89(27):270401, December 2002.
 - ³ Ali Mostafazadeh. Exact PT-Symmetry Is Equivalent to Hermiticity. *Journal of Physics A: Mathematical and General*, 36(25):7081–7091, June 2003. arXiv: quant-ph/0304080.
 - ⁴ Carl M. Bender. Making Sense of Non-Hermitian Hamiltonians. *Reports on Progress in Physics*, 70(6):947–1018, June 2007. arXiv: hep-th/0703096.
 - ⁵ Ingrid Rotter. A non-Hermitian Hamilton operator and the physics of open quantum systems. *Journal of Physics A: Mathematical and Theoretical*, 42(15):153001, April 2009.
 - ⁶ Ali Mostafazadeh. PSEUDO-HERMITIAN REPRESENTATION OF QUANTUM MECHANICS. *International Journal of Geometric Methods in Modern Physics*, 07(07):1191–1306, November 2010.
 - ⁷ Nimrod Moiseyev. *Non-Hermitian quantum mechanics*. Cambridge University Press, Cambridge; New York, 2011. OCLC: 705929219.
 - ⁸ K. G. Makris, R. El-Ganainy, D. N. Christodoulides, and Z. H. Musslimani. Beam Dynamics in P T Symmetric Optical Lattices. *Physical Review Letters*, 100(10):103904, March 2008.
 - ⁹ Christian E. Rter, Konstantinos G. Makris, Ramy El-Ganainy, Demetrios N. Christodoulides, Mordechai Segev, and Detlef Kip. Observation of paritytime symmetry in optics. *Nature Physics*, 6(3):192–195, March 2010.
 - ¹⁰ Alois Regensburger, Christoph Bersch, Mohammad-Ali Miri, Georgy Onishchukov, Demetrios N. Christodoulides, and Ulf Peschel. Paritytime synthetic photonic lattices. *Nature*, 488(7410):167–171, August 2012.
 - ¹¹ W D Heiss. The physics of exceptional points. *Journal of Physics A: Mathematical and Theoretical*, 45(44):444016, November 2012.
 - ¹² Kun Ding, Guancong Ma, Meng Xiao, Z. Q. Zhang, and C. T. Chan. Emergence, coalescence, and topological properties of multiple exceptional points and their experimental realization. *Phys. Rev. X*, 6:021007, Apr 2016.
 - ¹³ Ali Mostafazadeh. Pseudo-Hermiticity versus PT symmetry: The necessary condition for the reality of the spectrum of a non-Hermitian Hamiltonian. *Journal of Mathematical Physics*, 43(1):205–214, January 2002.
 - ¹⁴ Francesco Cannata, Georg Junker, and Johannes Trost. Schrödinger operators with complex potential but real spectrum. *Physics Letters A*, 246(3):219–226, September 1998.
 - ¹⁵ Eduard N. Tsoy, Izzat M. Allayarov, and Fatkhulla Kh Abdullaev. Stable localized modes in asymmetric waveguides with gain and loss. *Optics Letters*, 39(14):4215–4218, July 2014.
 - ¹⁶ K. G. Makris, Z. H. Musslimani, D. N. Christodoulides, and S. Rotter. Constant-intensity waves and their modulation instability in non-Hermitian potentials. *Nature Communications*, 6:7257, July 2015.
 - ¹⁷ Sean Nixon and Jianke Yang. All-real spectra in optical systems with arbitrary gain-and-loss distributions. *Physical Review A*, 93(3):031802, March 2016.
 - ¹⁸ Chao Hang, Gregory Gbadadze, and Guoxiang Huang. Realization of non-PT-symmetric optical potentials with all-real spectra in a coherent atomic system. *Physical Review A*, 95(2):023833, February 2017.
 - ¹⁹ Tuck C. Choy. *Effective Medium Theory: Principles and Applications*. Oxford University Press, December 2015. Google-Books-ID: sHUGcWAAQBAJ.
 - ²⁰ D. Dragoman. Complex conjugate media: Alternative configurations for miniaturized lasers. *Optics Communications*, 284(8):2095–2098, April 2011.
 - ²¹ Amjad Imran and Ahsan Illahi. On the Effects of Complex Conjugate Medium on TM Scattering by a Strip. *Journal of Electromagnetic Analysis and Applications*, 03(07):267–270, 2011.
 - ²² A. Basiri, I. Vitebskiy, and T. Kottos. Light scattering in pseudopassive media with uniformly balanced gain and loss. *Physical Review A*, 91(6):063843, June 2015.
 - ²³ Ping Bai, Kun Ding, Gang Wang, Jie Luo, Zhao-Qing Zhang, C. T. Chan, Ying Wu, and Yun Lai. Simultaneous realization of a coherent perfect absorber and laser by zero-index media with both gain and loss. *Physical Review A*, 94(6):063841, December 2016.
 - ²⁴ Yadong Xu, Yangyang Fu, and Huanyang Chen. Electromagnetic wave propagations in conjugate metamaterials. *Optics Express*, 25(5):4952, March 2017.
 - ²⁵ Xueqin Huang, Yun Lai, Zhi Hong Hang, Huihuo Zheng, and C. T. Chan. Dirac cones induced by accidental degeneracy in photonic crystals and zero-refractive-index materials. *Nature Materials*, 10(8):582–586, August 2011.
 - ²⁶ Bo Zhen, Chia Wei Hsu, Yuichi Igarashi, Ling Lu, Ido Kaminer, Adi Pick, Song-Liang Chua, John D. Joannopoulos, and Marin Soljai. Spawning rings of exceptional points out of Dirac cones. *Nature*, 525(7569):354–358, September 2015.
 - ²⁷ Kazuaki Sakoda. *Optical properties of photonic crystals*. Number 80 in Springer series in optical sciences. Springer, Berlin ; New York, 2nd ed edition, 2005.
 - ²⁸ Kun Ding, Z. Q. Zhang, and C. T. Chan. Coalescence of exceptional points and phase diagrams for one-dimensional P T -symmetric photonic crystals. *Physical Review B*, 92(23):235310, December 2015.
 - ²⁹ Kazuaki Sakoda. Proof of the universality of mode symmetries in creating photonic Dirac cones. *Optics Express*, 20(22):25181, October 2012.
 - ³⁰ Alexander Szameit, Mikael C. Rechtsman, Omri Bahat-Treidel, and Mordechai Segev. P T -symmetry in honeycomb photonic lattices. *Physical Review A*, 84(2):021806, August 2011.
 - ³¹ Andrei Andryieuski, Sangwoo Ha, Andrey A. Sukhorukov, Yuri S. Kivshar, and Andrei V. Lavrinenko. Bloch-mode analysis for retrieving effective parameters of metamaterials. *Physical Review B*, 86(3):035127, July 2012.
 - ³² Marcelo Davanco, Yaroslav Urzhumov, and Gennady Shvets. The complex Bloch bands of a 2d plasmonic crystal displaying isotropic negative refraction. *Optics Express*, 15(15):9681, 2007.